Available online at www.sciencedirect.com

ScienceDirect

Energy Procedia 78 (2015) 537 – 542

Energy Procedia

6th International Building Physics Conference, IBPC 2015

Characterization of fibrous insulating materials in their application in Dynamic Insulation technology

Andrea Alongi[a,*], Livio Mazzarella[a]

[a]*Politecnico di Milano, Dipartimento di Energia, via Lambruschini 4, Milano 20156, Italy*

Abstract

Previous studies dealing with dynamic insulation technology neglect the microscopic interaction between the solid matrix of the porous material and the air flowing through the pore structure. The main goal of this work is to investigate this interaction, and its effects on the heat transfer phenomena at macroscopic scale using the Volume Average Method. At first, the microscopic geometry of two samples of rock wool is investigated through image analysis, leading to the evaluation of porosity and granulometry. Then, the volume averaging technique is applied to the microstructure of fibrous materials. Thermal dispersion and thermal tortuosity are introduced and evaluated through numerical simulations of simplified geometry in laminar and low-Pe conditions, and two regression equations are defined.

Peer-review under responsibility of the CENTRO CONGRESSI INTERNAZIONALE SRL

Keywords: porous material, dynamic insulation, fibrous material, image analysis, local volume averaging

1. Introduction

The growing interest to the energy use reduction in buildings has led to the development, since the early Nineties, of new envelope technologies like the so called dynamic insulation system [1]. It is a technical solution based on the integration between ventilation plant and building structures, and works as follows: instead of being delivered or extracted through ducts or openings, ventilation air is forced to go slowly through dedicated building envelope porous walls, which consequently act as heat exchangers [1] and filters [2] of the ventilation system. Walls performance can also be controlled by changing air flow rate and direction. In fact, they both affect the

* Corresponding author. Tel.: +39 02 2399 3867; fax: +39 02 2399 3868.
E-mail address: andrea.alongi@polimi.it

Peer-review under responsibility of the CENTRO CONGRESSI INTERNAZIONALE SRL
doi:10.1016/j.egypro.2015.11.732

Nomenclature

A_{sf}	interface between fluid and solid phase [m^2]
c_p	thermal capacity by mass at constant pressure [J/(kg K)]
$\mathbf{K_{eff}}$	effective thermal conductivity tensor (2-by-2) [W/(m K)]
$\mathbf{K_{disp}}$	thermal dispersion tensor (2-by-2) [W/(m K)]
$\mathbf{K_{tor}}$	thermal tortuosity tensor (2-by-2) [W/(m K)]
k_f, k_s	thermal conductivity of fluid and solid phase [W/(m K)]
L_{REV}	REV characteristic dimension [m]
$\mathbf{n}_{sf}$	local coordinate normal to A_{sf} ($\mathbf{n}_{sf} = n_{sf,x} \cdot \mathbf{i} + n_{sf,y} \cdot \mathbf{j}$)
Pe	Peclet number [-] ($Pe = u \cdot L_{REV} \left(\rho c_p\right)_f \cdot k_f^{-1}$)
T	temperature distribution [K]
$\mathbf{u}$	local velocity vector [m/s] ($\mathbf{u} = u \cdot \mathbf{i} + v \cdot \mathbf{j}$)
V_{REV},V_f	REV and fluid phase volume [m^3]

Greek symbols

ε	volume fraction of fluid phase (porosity) [-]
ρ	mass density [kg/m^3]

equivalent thermal transmittance [1,3]. Moreover, the comparison between velocity field and thermal flux directions allows us to identify two working conditions: *pro-flux* condition, if air velocity and thermal flux have the same direction; *contra-flux* condition in the opposite case.

The main goal of this work is to investigate the interaction between the solid matrix and the air flow at a microscopic level inside rock wool materials, since it has been neglected in previous works. Therefore, heat transfer is analyzed using the volume average method: the micro-scale geometry is investigated through image analysis; then, CFD simulations are performed to the temperature distribution and the velocity field at fiber-scale level.

2. The Volume Average Method

In previous work, the evaluation of the temperature profile in a porous layer crossed by flowing air was done considering the heat transfer phenomenon both in dynamic [4] and in steady state conditions [3]. Moreover, an equation for the effective thermal transmittance was given [1, 3], as a function of the air velocity and the stationary thermal resistance of the porous layers involved. It is important to remark that thermal conductivity involved in all the equations is usually the nominal value of the used material (i.e. as given by datasheets in reference conditions). This introduces an implicit simplification, by neglecting the macroscopic effects of the microscopic interaction between the moving fluid and the solid part of the porous medium (contact surface, geometry, convective heat exchange, etc.).

In order to investigate more in detail the heat transfer phenomenon, a useful method is the Volume Average technique, which is described in [5, 6]. This approach is based on specific averaging technique applied to the energy equations that describe the temperature distribution in the fluid and the solid phases of a porous medium. For the sake of brevity, the description of intermediate calculations is omitted and only the resulting equations, describing the temperature distribution in a porous medium in a macroscopic scale, are reported:

$$\left[\varepsilon \cdot \left(\rho c_p\right)_f + (1-\varepsilon) \cdot \left(\rho c_p\right)_s\right] \frac{\partial \langle T \rangle}{\partial} + \varepsilon \cdot \left(\rho c_p\right)_f \cdot \langle \mathbf{u} \rangle^f \cdot \nabla \langle T \rangle = \nabla \cdot (\mathbf{K_{eff}} \cdot \nabla \langle T \rangle) \tag{1}$$

B.C.: $\tilde{T}_f = \tilde{T}_s = \tilde{T}$ and $\mathbf{n}_{sf} \cdot k_f \quad \nabla \langle \ \rangle = \quad \langle \ \rangle$ on A_{sf} (2)

where ε is the porosity, defined as the volume fraction of the fluid phase evaluated over the *Representative Elementary Volume* (*REV*), which is defined in [5, 6], $\langle\ \rangle$ and ˜ operators are respectively the volume average of a

quantity over the REV and its local deviation. A detailed description can be found in [5, 6]. For what concerns the conductive term in Eq. (1), thermal conductivity tensor is defined as follows:

$$\mathbf{K_{eff}} = \left[\varepsilon \cdot k_f + (1-\varepsilon \cdot k_s)\right] \cdot \mathbf{I} + \mathbf{K_{tor}} + \mathbf{K_{disp}} = \langle k \rangle \cdot \mathbf{I} + \mathbf{K_{tor}} + \mathbf{K_{disp}} \tag{3}$$

where **I** is the 2-by-2 identity matrix; $\mathbf{K_{tor}}$ and $\mathbf{K_{disp}}$ are respectively the thermal tortuosity and the thermal dispersion tensors (both 2-by-2), and can be defined as a consequence of the averaging process over the REV:

$$\mathbf{K_{tor}} \cdot \nabla \langle T \rangle = \frac{k - k_s}{V_{REV}} \int_{A_{sf}} \mathbf{n} \cdot \mathbf{i} T \, dA \;\Rightarrow\; k_{tor,xx} = \frac{(k_f - k_s) V_{REV}}{\Delta \langle T \rangle_x / L_{REV}} \int_{A_{sf}} n_{fs,x} \cdot (T - \langle T \rangle) \, dA \tag{4}$$

$$\mathbf{K_{disp}} \cdot \nabla \langle T \rangle = \frac{(\rho c_p)_f}{V_{REV}} \int_{V_f} \mathbf{u} \mathbf{i} T \cdot dV \;\Rightarrow\; \langle T \rangle = \frac{(\rho c_p)_f / V_{REV}}{\Delta \langle T \rangle_x / L_{REV}} \int_{V_f} (u - \langle u \rangle) \cdot (T - \langle T \rangle) \, dV \tag{5}$$

where the subscript *f* means that quantities are integrated only over the fluid phase volume (V_f) of the REV. According to Eqs. (4) and (5), the microscopic interaction between fluid and solid matrix of a porous medium is taken into account at macroscopic level, because both equations depend on the spatial distribution of deviations from the volume average value of a quantity (e.g. T and **u**). Furthermore, considering a multidimensional heat transfer phenomenon, thermal dispersion and tortuosity are written in tensor form. If our analysis of the building envelope is restricted to a one dimensional problem, which is generally enough, these quantities become scalar. With this assumption, the longitudinal component of thermal tortuosity and dispersion are reported in Eqs. (4) and (5), where *u* is the x-component of the local velocity vector. To solve integrals in Eqs. (4) and (5) the spatial distributions of local deviations are needed. In order to derive such functional relationships, velocity and temperature fields have been evaluated with CFD simulations, building a model based on the micro-structural features of rock wool real samples, obtained through mathematical morphology and image analysis.

3. Characterization of the micro-scale geometry of rock wool

The first step in the application of the volume average method to fibrous material is the definition of the REV, both in terms of size and microscopic geometry. Therefore, two samples (S1 and S2, with density of 50 kg/m^3 and 100 kg/m^3 respectively) of rock wool are investigated through image analysis, obtaining the porosity range and the granulometry distribution. Each sample is cut into slices, along the three main Cartesian planes, obtaining thin sections of the material (10 for each plane) which are photographed through a microscope with a 200x enlargement (Fig. 1 up). In this way, 30+30 images are produced, covering an area of 519μm x 389μm with each picture. All images have then been converted into a binary representation (Fig. 1 down): in this way, the fluid phase is black, while the solid part is white. Then, they have been used for further calculations.

3.1. Porosity

Introducing a phase function Z(**r**), which is equal 1 if a point belongs to the fluid phase of the domain, or 0 if it is located in the solid region [6, 7], porosity can be defined as the surface average of the phase function over the REV. Every image has been scanned with square modules with various dimensions (side equal to 1536 pxl, 1024 pxl, 768 pxl, 576 pxl, 512 pxl, 432 pxl, 324 pxl, 256 pxl, 240 pxl and 128 pxl), then porosity is evaluated for each subsample and for the overall image (2048 pxl x 1536 pxl).

Table 1: average porosity calculated for samples S1 and S2. Maximum, minimum and the standard deviation of records are reported.

	Sample S1			Sample S2		
	Plane A	**Plane B**	**Plane C**	**Plane A**	**Plane B**	**Plane C**
average	97.12%	96.58%	96.09%	95.83%	94.25%	95.44%
standard deviation	±1.39%	±1.16%	±1.32%	±1.22%	±2.41%	±1.72%
minimum	94.77%	94.37%	94.03%	94.13%	87.78%	92.70%
maximum	98.51%	97.93%	98.00%	97.36%	96.55%	97.64%

Considering the overall images, results reported in Table 1 show a high porosity level (generally over 94%), with little dispersion around the average (standard deviation below 2.5%). Moreover, S1 shows slightly higher average porosity (likely ascribable to different densities), while no significant dependence on the cutting plane is found. This means that, considering void fraction, there is no preferential direction of the fiber deposition in the solid matrix.

Dealing now with the definition of the REV size, it has been assumed as the smallest sub-sample dimension which shows a ratio between the standard deviation and the average of porosity below 5%. This means that, from a statistical point of view, volumes of material of the chosen size have similar void fraction. This value is generally lower than 256pxl (around 64μm), even if some outliers have been found (more irregular microstructures).

3.2. Granulometry distribution

The algorithm for the evaluation of the granulometry distribution from an image is based on the mathematical morphology principles [7, 8], and leads to the evaluation of the frequency distribution that represents the amount of pixels, inside the investigated image, that belong to fibers of a given radius. In this work, radiuses have been investigated in a range from 1 pxl to 200 pxl (0.25 μm÷50.76 μm). This analysis has been performed for all images, and then granulometry distributions have been averaged for the A, B and C planes of both samples, in order to filter non-significant peculiarities of the individual images and emphasize any possible general feature. Frequency distributions reported in Fig. 2 show that the most part of fibers radius statistically lies in a range between 2.5 μm and 10 μm (from 10pxl to 40pxl), even if bigger fibers are present.

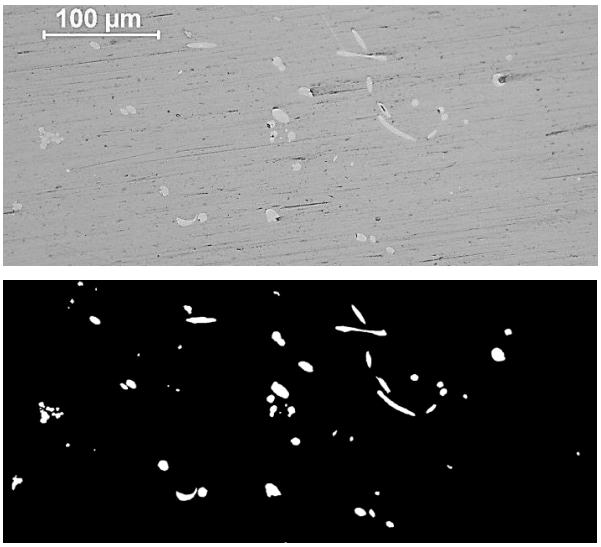

Fig. 1: example of a microscopic image of a rock wool sample, both in its original (up) and binary (down) version.

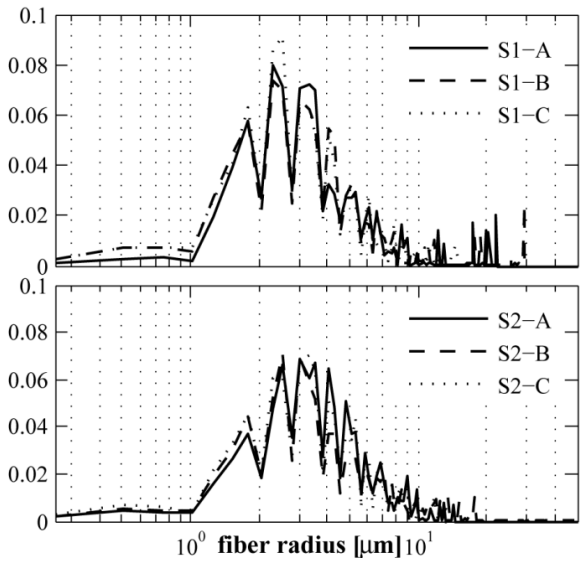

Fig. 2: frequency distribution of fiber diameters for sample S1 (up) and S2 (down).

4. Numerical simulations of simplified geometry

4.1. Domain definition and boundary conditions

The microscopic geometry of fibrous insulating materials has been simplified, representing fibers as parallel cylinders with constant diameter (5μm), orthogonally displaced to the two-dimensional CFD simulation plane (Fig. 3). The effects of void fraction have been investigated, considering five possible levels (80%, 85%, 90%, 95% and 99%) which have been chosen according to the analyses presented in the previous section. Due to the simplicity of the geometry, different porosity levels have been obtained keeping constant the fiber cross-section and varying L_{REV} (refer to Fig. 3 for the definition). Thermo physical properties of the materials used for simulations are listed in

Table 2. Since this work is focused on building material like rock wool, basaltic rock properties have been used to describe the solid matrix. Energy and momentum equations have been solved over the fluid and the solid phases in steady-state condition using a finite volume discretization method. No viscous model is involved, because of the low Re condition, resulting from low values of inlet air velocity. This condition leads also to low values of Pe number.

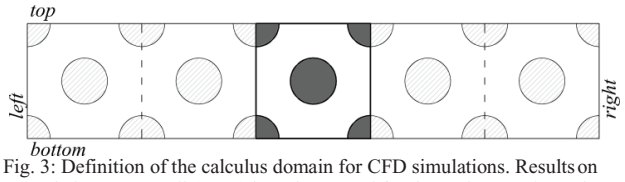

Fig. 3: Definition of the calculus domain for CFD simulations. Results on central elementary cell (REV) have been used for thermal tortuosity and dispersion evaluation. L_{REV} is assumed to be equal to the side of the square-shaped REV.

Table 2: Thermophysical properties of fluid and solid matrix

Fluid: Air	
density - ρ_f	1.225 kg/m^3
conductivity - k_f	0.024 W/m K
specific heat – $c_{p,f}$	1006 J/kg K
Solid: Basaltic Rock	
density - ρ_s	2870 kg/m^3
conductivity - k_s	1.75 W/m K
specific heat – c_s	910 J/kg K

Dealing with boundary conditions, five steps of average inlet velocity (0.001 m/s, 0.003 m/s, 0.005 m/s, 0.007 m/s and 0.01 m/s) have been applied to the inlet section on the unit-cell left side. Pe number has been successively calculated according to its definition given in [5, 6]. A temperature gradient has also been imposed over the x coordinate (2500 K/m and 500 K/m – hereafter addressed as ΔT_1 and ΔT_2 - which are calculated considering a temperature difference of 25 K and 5 K across a slab with a 1 cm thickness). The central REV has been considered for further calculation. Symmetry condition has been taken into account for both top and bottom faces of the computational domain.

4.2. Results and discussion

An amount of 50 simulations has been performed, and results have been post-processed to calculate thermal tortuosity and dispersion using the discrete form of Eqs. (4) and (5). The analysis of results has shown a negligible dependence on temperature gradient, as it is displayed in Table 3 and Table 4: thermal tortuosity values distribution shows small values of standard deviation for every void fraction considered; results obtained for thermal dispersion with the two temperature difference assumed display an absolute difference which is from one to three orders of magnitude smaller than the quantity itself. Therefore, all results obtained for different thermal boundary condition are averaged for further calculations. Moreover, as far as the thermal tortuosity is concerned, seems to be not affected by the velocity boundary conditions either, while changes significantly from a void fraction to the other.

Table 3: Results of thermal tortuosity calculation. For every porosity level and every working configuration minimum and maximum values are reported. Arithmetic mean (μ) and standard deviation (σ) are given.

ε	**min.**	**max.**	μ	σ
80%	6.16%	6.81%	6.48%	0.31%
85%	7.48%	7.54%	7.50%	0.02%
90%	9.50%	9.55%	9.52%	0.01%
95%	13.02%	13.09%	13.06%	0.02%
99%	24.65%	25.29%	25.00%	0.22%

Table 4: Comparison among different thermal dispersion values depending on temperature difference between left and right edge of the considered REV.

		thermal dispersion		
ε	**u [m/s]**	ΔT_1	ΔT_2	**abs. diff.**
80%	0.001	2.26 10^{-8}%	1.49 10^{-8}%	7.65 10^{-9}%
	0.01	2.37 10^{-6}%	2.43 10^{-6}%	5.21 10^{-8}%
99%	0.001	1.90 10^{-6}%	1.94 10^{-6}%	3.33 10^{-8}%
	0.01	2.11 10^{-4}%	2.11 10^{-4}%	2.85 10^{-7}%

Starting from the assumption that both quantities depend on parameter like porosity, horizontal temperature gradient and Peclet number, it has been possible to evaluate two regression equations based on the numerical results of CFD simulations. In Figure 4 and Figure 5 both quantities are represented as a fraction of the average thermal conductivity $\langle k \rangle$ of the REV, according to its definition given in Eq. (3). Interpolating equations for both these ratios are:

$$\frac{k_{tort,xx}}{\langle k \rangle} \approx -0.188 \cdot \frac{0.814 + \sum^{55}}{\varepsilon^{-4.5}} \qquad (6)$$

$$\frac{k_{disp,xx}}{\langle k \rangle} \approx 2.808 \cdot 10^{-4} \cdot Pe^2_{L_{REV}} \cdot e^{-5.364 \cdot \frac{(1-\varepsilon)}{\varepsilon}} \qquad (7)$$

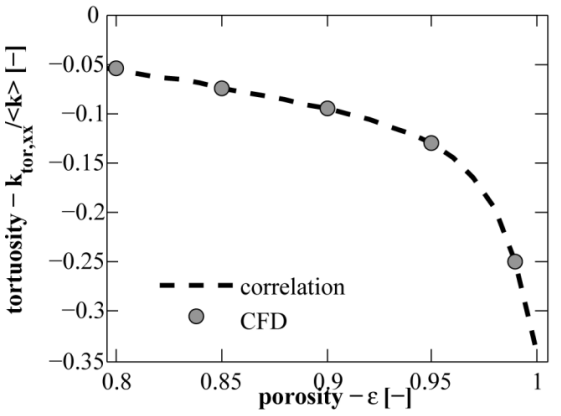

Figure 4: Comparison between numerical results and regression curves for the thermal tortuosity coefficient $k_{tor,xx}/\langle k \rangle$.

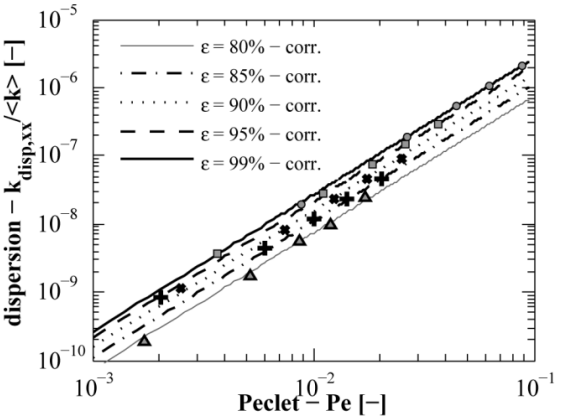

Figure 5: Comparison between numerical results and regression curves for the thermal dispersion coefficient $k_{disp,xx}/\langle k \rangle$.

As stated before, thermal tortuosity (Figure 4) is affected only by porosity. Moreover, its relevance increases for higher void fractions, which are typical for fibrous insulating material in buildings, as it has been proved previously: within the void fraction range from 90% to 99%, thermal tortuosity is approximately between 9.5% and 25% of the average thermal conductivity. Considering Figure 5, where thermal dispersion is represented, it is possible to observe that its contribution on the energy balance is very small in the low Pe region (maximum $2.1 \cdot 10^{-4}$% of the correspondent average thermal conductivity). Therefore, under these conditions, this quantity can be neglected.

5. Conclusions and future development

All analyses shown in this work are aimed at the investigation of the heat exchange between the flowing air and the solid matrix at microscopic scale of a porous medium. This could provide a better comprehension of the thermal behavior of dynamic insulation in building envelopes. For this reason, the volume average method has been used, leading to an averaged equation for heat transfer, along with the definition thermal tortuosity and dispersion. First, the solid matrix has been investigated through image analysis of rock wool samples: the porosity range has been assessed to be from 88% to 98% (average ~96%); then, image granulometry has shown that fiber radius is generally smaller than 5μm, even if bigger fibers have been found (radius ~30μm). In the second part of the work, several numerical simulations of simplified geometry have been performed to calculate thermal tortuosity and dispersion, considering five values of intrapore air velocity, five void fractions and two temperature differences. Concerning the thermal tortuosity, it is only dependent on porosity, and seems to have an important impact on the effective thermal conductivity. Conversely, thermal dispersion appears to be negligible: it depends both on porosity and Pe number, but its order of magnitude is generally lower than the 10^{-4}% of the volume average thermal conductivity.

References

[1] Imbabi MS-E. A passive–active dynamic insulation system for all climates. Int. J. Sust. Built Env. 2013;1: 247–258.
[2] Taylor BJ, Webster R, Imbabi MS. The building envelope as an air filter. Build. Environ. 1999;34: 353-361.
[3] Taylor BJ, Cawthorne DA, Imbabi MS. Analytical investigation of the steady-state behaviour of dynamic and diffusive building envelopes. Build. Environ. 1996;31:6 519-525.
[4] Dimoudi A, Androutsopoulos A, Lykoudis S. Experimental work on a linked, dynamic and ventilated, wall component. Energ. Buildings. 2004; 36: 443-453.
[5] Quintard M, Whitaker S. Theorethical analysis of transport in porous media. In: Vafai K, editors. Handbook of porous media. New York: Marcel Dekker Inc. 2000. p. 1-52.
[6] Kaviany M. Principles of Heat Transfer in Porous Media. 2nd ed. New York: Springer; 1995.
[7] Lux J, Ahmadi A, Gobbé C, Delisée C. Macroscopic thermal properties of real fibrous materials: volume averaging method and 3D image analysis. Int. J. Heat Mass Tran. 2006;49: 1958-1973.
[8] Serra J. Image analysis and mathematical morphology. London: Academic Press Inc; 1982.